Dynamic feature of mitotic arrest deficient 2–like protein 2 (MAD2L2) and structural basis for its interaction with chromosome alignment–maintaining phosphoprotein (CAMP)

Received for publication, June 28, 2017, and in revised form, September 4, 2017 Published, Papers in Press, September 8, 2017, DOI 10.1074/jbc.M117.804237

Kodai Hara (原 幸大)[‡], Shota Taharazako (田原迫 奨大)[‡], Masanori Ikeda (池田 真教)[§], Hiroki Fujita (藤田 拡樹)[§], Yoshiko Mikami (三上 嘉子)[§], Sotaro Kikuchi (菊池 壮太郎)[‡], Asami Hishiki (菱木 麻美)[‡], Hideshi Yokoyama (横山 英志)[¶], Yoshinobu Ishikawa (石川 吉伸)[‡], Shin-ichiro Kanno (菅野 新一郎)[§], Kozo Tanaka (田中 耕三)[§], and Hiroshi Hashimoto (橋本 博)[‡1]

From the [‡]School of Pharmaceutical Sciences, University of Shizuoka, 52-1 Yada, Suruga-ku, Shizuoka, Shizuoka 422-8002, Japan, [§]Institute of Development, Aging, and Cancer, Tohoku University, 4-1 Seiryo-cho, Aoba-ku, Sendai, Miyagi 980-8575, Japan, and [¶]Faculty of Pharmaceutical Sciences, Tokyo University of Science, 2641 Yamazaki, Noda, Chiba 278-8510, Japan

Edited by Patrick Sung

Mitotic arrest deficient 2–like protein 2 (MAD2L2), also termed MAD2B or REV7, is involved in multiple cellular functions including translesion DNA synthesis (TLS), signal transduction, transcription, and mitotic events. MAD2L2 interacts with chromosome alignment–maintaining phosphoprotein (CAMP), a kinetochore-microtubule attachment protein in mitotic cells, presumably through a novel "WK" motif in CAMP. Structures of MAD2L2 in complex with binding regions of the TLS proteins REV3 and REV1 have revealed that MAD2L2 has two faces for protein–protein interactions that are regulated by its C-terminal region; however, the mechanisms underlying the MAD2L2–CAMP interaction and the mitotic role of MAD2L2 remain unknown. Here we have determined the structures of human MAD2L2 in complex with a CAMP fragment in two crystal forms. The overall structure of the MAD2L2–CAMP complex in both crystal forms was essentially similar to that of the MAD2L2–REV3 complex. However, the residue interactions between MAD2L2 and CAMP were strikingly different from those in the MAD2L2–REV3 complex. Furthermore, structure-based interaction analyses revealed an unprecedented mechanism involving CAMP's WK motif. Surprisingly, in one of the crystal forms, the MAD2L2–CAMP complex formed a dimeric structure in which the C-terminal region of MAD2L2 was swapped and adopted an immature structure. The structure provides direct evidence for the dynamic nature of MAD2L2 structure, which in turn may have implications for the protein–protein interaction mechanism and the multiple functions of this protein. This work is the first structural study of MAD2L2 aside from its role in TLS and might pave the way to clarify MAD2L2's function in mitosis.

This work was supported by JSPS KAKENHI Grants 25291017 and 16H04755, MEXT KAKENHI Grants 25121728 and 17H06014, The Takeda Science Foundation and Naito Foundation (to H. H.), JSPS KAKENHI Grants 15K18491 and 17K07314 (to K. H.), and JSPS KAKENHI Grant 15H04368, MEXT KAKENHI Grant 16H01296, and a grant from the Takeda Science Foundation (to K. T.). The authors declare that they have no conflicts of interest with the contents of this article.

The atomic coordinates and structure factors (codes 5XPT and 5XPU) have been deposited in the Protein Data Bank (http://wwpdb.org/).

[1] To whom correspondence should be addressed. Tel./Fax: 81-54-264-5644; E-mail: hash@u-shizuoka-ken.ac.jp.

Vital cellular functions are highly regulated by numerous protein–protein interactions (PPIs),[2] which are essentially target-specific processes that take place via one-to-one communication. In contrast, some proteins play the role of a "hub" or "adaptor" within a PPI network by having two or more interacting partners. MAD2L2 (also known as REV7 or MAD2B), a small protein comprising just 211 amino acid residues in human and including the HORMA (Hop1, Rev7, and Mad2) domain (Fig. 1), interacts with many partners and is crucially involved in diverse cellular functions, including translesion DNA synthesis (TLS) and mitotic events.

MAD2L2 was originally identified in studies of a yeast *rev7* mutant deficient in DNA damage-induced mutagenesis by UV (1–3), where the yeast Rev7 protein was identified as a regulatory component of DNA polymerase ζ (Pol-ζ), an error-prone DNA polymerase specialized in TLS (4). Human MAD2L2 has been shown to interact with REV3, a catalytic component of Pol-ζ (5), and also REV1, a binding scaffold in TLS (6, 7). The crystal structure of MAD2L2 in complex with a REV3 fragment revealed that MAD2L2 interacts with REV3 through its C-terminal region, termed the "safety belt," and also implied that a second PPI site for interaction with REV1 is induced on the C-terminal β-sheet of MAD2L2 by REV3 binding (8). Furthermore, crystal structures of higher order complexes including MAD2L2 have clarified the role of MAD2L2 as an adaptor protein with two PPI faces that enable it to regulate the recruitment of Pol-ζ to the damage site in TLS (9–12).

In addition to its well established function in TLS, several reports have suggested that MAD2L2 has a role in mitosis. Due to its sequence similarity with MAD2 (also termed MAD2A or MAD2L1), a spindle assembly checkpoint protein that interacts with CDC20 to inhibit the activity of the APC/C ubiquitin ligase, MAD2L2 was proposed to interact with CDH1 and thereby to function as an APC/C inhibitor (13–15); however, its distinct localization in mitotic cells away from CDH1 and the

[2] The abbreviations used are: PPI, protein–protein interaction; HORMA, Hop1, Rev7, and Mad2; TLS, translesion DNA synthesis; Pol, polymerase; CAMP, chromosome alignment–maintaining phosphoprotein; IMAC, immobilized metal affinity chromatography; IF, immunofluorescence; WB, Western blotting; IP, immunoprecipitation.

phenotype caused by its depletion imply that MAD2L2 is more likely to be engaged in spindle formation and chromosome alignment (16). Indeed, the physical interaction of MAD2L2 with RAN, an important protein of bipolar spindle formation, has also been reported (17).

A zinc finger protein ZNF828 was also identified as a MAD2L2-binding protein (18, 19) and was subsequently characterized as CAMP (chromosome alignment–maintaining phosphoprotein; also termed CHAMP1), a protein responsible for maintaining kinetochore-microtubule attachment in mitotic cells (19). Furthermore, it has been recently reported that CAMP is associated with a severe developmental disorder (20), and mutations in CAMP cause global development delay, intellectual disability, and dysmorphic facial features (21–23). Therefore, the structure of CAMP and its PPI has considerable interest in the context of biomedical sciences and clinical investigations.

Human CAMP consists of 812 amino acid residues containing C2H2-Zn finger domains (C2H2-ZNFs) and three characteristic repeats termed the WK, SPE, and FPE motifs (Fig. 1*A*); it interacts with MAD2L2 through its central region (residues 271–490) containing multiple WK motifs (19), implying that this motif has a crucial involvement in MAD2L2 binding. The WK motif is not present in the MAD2L2-binding region of either REV3 or REV1; thus, the structural basis of MAD2L2–CAMP interaction remains unknown. To date, structural studies of MAD2L2 have been limited to its complexes associated with TLS rather than those associated with its mitotic function; in addition, it is of interest to clarify the structural basis of the various PPIs of MAD2L2. In this study, therefore, the crystal structure of human MAD2L2 in complex with a CAMP fragment was determined. To our knowledge this is the first structure of an MAD2L2 complex associated with mitosis. It clarifies the mechanism underlying the MAD2L2–CAMP interaction involving the WK motif of CAMP. Furthermore, two different crystal structures indicate the dynamic nature of the C-terminal region of MAD2L2, providing direct evidence for the conformational changes of MAD2L2 together with the associated functional implications.

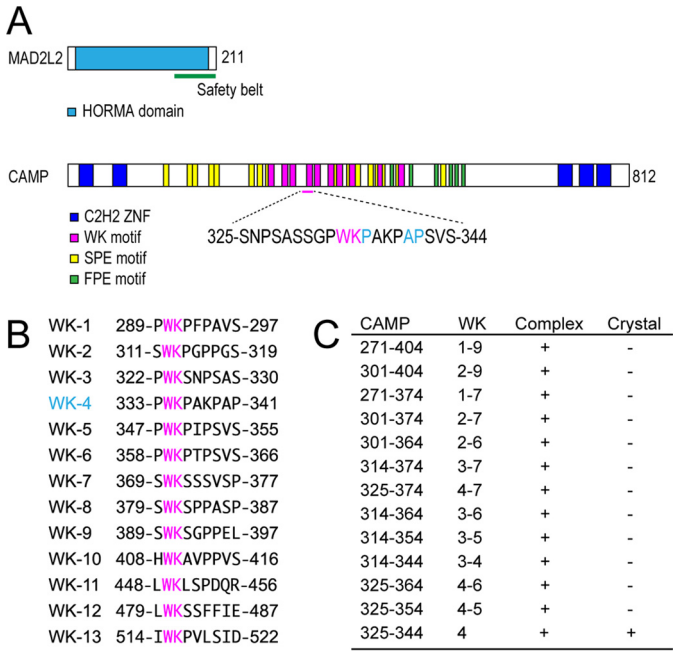

Figure 1. Domain architectures and interaction of human MAD2L2 and CAMP. *A*, human MAD2L2 comprises 211 amino acid residues (*upper panel*). The HORMA domain is shown by a *light blue rectangle*. The C-terminal region of MAD2L2 (residues 153–211), termed the safety belt, is indicated by the *green line*. Human CAMP comprises 812 amino acid residues (*lower panel*). C2H2-Zn finger domains (*C2H2 ZNFs*), WK, SPE, and FPE motifs are shown by *blue*, *magenta*, *yellow*, and *green rectangles*, respectively (19). The region used in this crystallographic study is indicated by the *magenta line below the domain diagram* together with its amino acid sequence (residues 325–344). *B*, WK sequences of human CAMP. Human CAMP has 13 WK sequences designated WK-1 ~ WK-13. For clarification, tryptophan and lysine residues are colored in *magenta*. The WK-4 responsible for MAD2L2 interaction is highlighted in *light blue*. *C*, result of co-purification of MAD2L2–CAMP complex. The first column (*CAMP*) shows amino acid residues of CAMP fragment used. The second column (*WK*) shows WK sequence in the CAMP fragment. The third column (*Complex*) shows results of co-purification of the complex. The symbol + indicates success in co-purification. The forth column (*Crystal*) shows results of crystallization. The symbols + and − indicate success and failure in crystallization of the complex, respectively.

Results

Structure of the MAD2L2–CAMP complex

CAMP has 13 WK sequences (Fig. 1*B*). Of these the region containing WK-1~WK-12 has been shown to interact with MAD2L2 (19). To identify the WK sequence responsible for MAD2L2 binding and to optimize the MAD2L2-binding region for the crystallographic study, we performed co-purification of MAD2L2 in complex with a CAMP fragment by immobilized metal affinity chromatography (IMAC) (Fig. 1*C*). Consequently, MAD2L2 in complex with a CAMP fragment containing WK-4 (residues 325–344; Fig. 1) was successfully crystallized. Crystals of human MAD2L2 in complex with the CAMP fragment were obtained in two crystal forms, Form-I and Form-II, and structures of the MAD2L2–CAMP complex in these crystals were determined at 2.1 and 2.3 Å resolution, respectively. The MAD2L2–CAMP complex adopted a monomeric structure in the Form-I crystal (Fig. 2*A*), whereas unexpectedly it formed a dimeric structure through exchange of the C-terminal region of MAD2L2 and the region adopted an immature structure in the Form-II crystal (Fig. 2*B*). Although structural differences of MAD2L2 were observed in the two complexes (Fig. 2*C*), the interactions between MAD2L2 and CAMP were essentially identical in both complexes. Therefore, the structure and interactions of the MAD2L2–CAMP complex in the Form-I crystal are described here, and the Form-II structure of the MAD2L2–CAMP complex is described below.

The crystal structure of the MAD2L2–CAMP complex comprises four α-helices (αA~αD), eight β-strands (β2~β8′′), and 3_{10} helices (Fig. 2, *A* and *C*). As previously observed in the structure of the MAD2L2–REV3 complex (8), the CAMP fragment is wrapped in the C-terminal region of MAD2L2 termed the safety belt, which was originally noted in the MAD2–MAD1 complex (24). The structures of MAD2L2 bound to CAMP and REV3 are basically identical except for the β5-αC region and the N terminus (Fig. 2*D*). These regions also differ between the Form-I and Form-II structures (Fig. 2*C*); thus, they might be correlated with dynamic features of the protein, as described below. Similar to MAD2L2, the main-chain atoms of CAMP and REV3 can be closely superimposed, indicating that overall

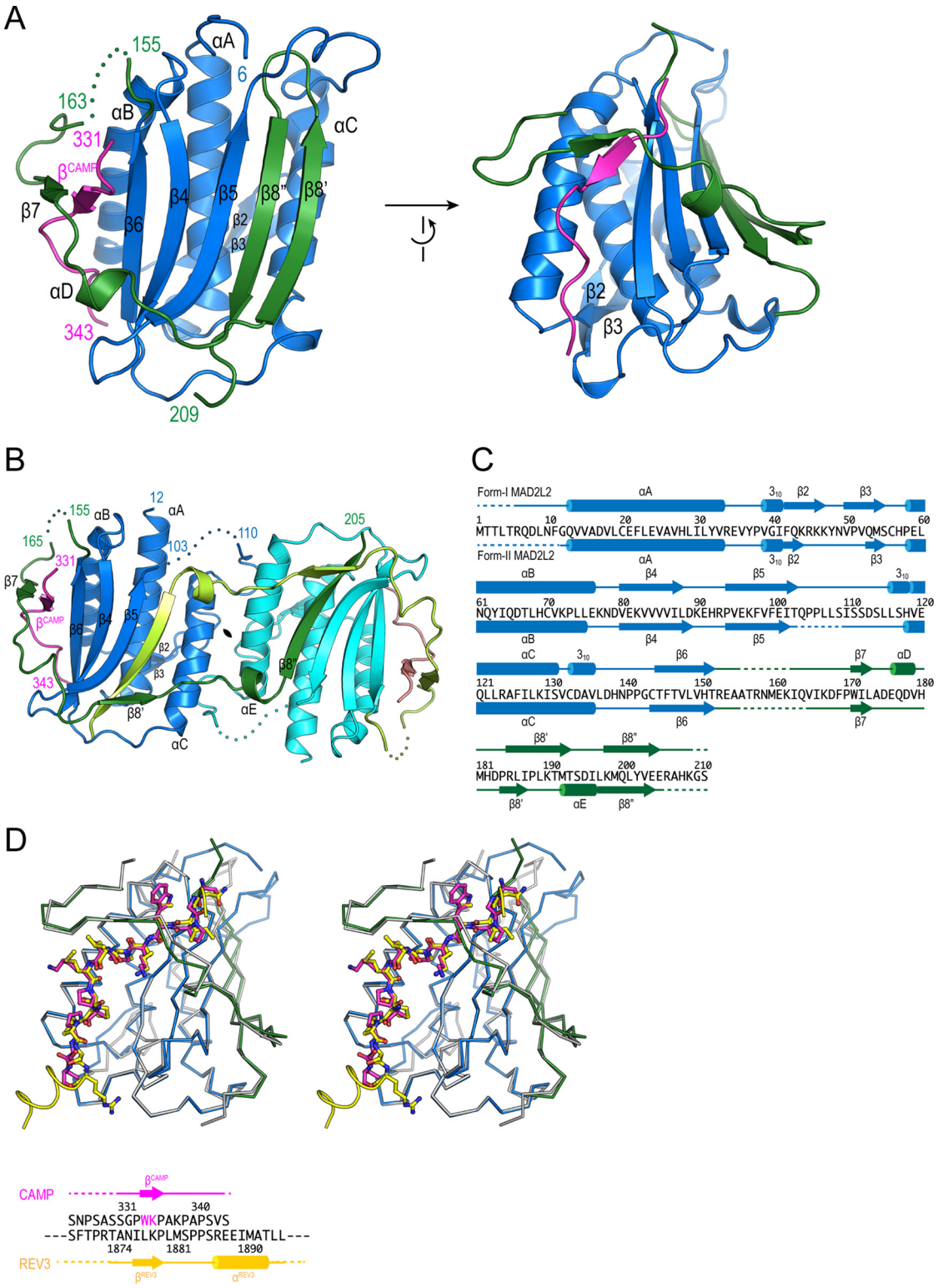

Figure 2. Structures of MAD2L2 in complex with a CAMP fragment. *A*, form-I structure of the MAD2L2–CAMP complex. MAD2L2 is shown in *blue* and *green* (safety belt), and the CAMP fragment is shown in *magenta*. The residue numbers of termini in the defined structure are labeled. The disordered region (residues 156–162) is shown by *green dots*. Secondary structures are labeled. *B*, form-II structure of the MAD2L2–CAMP complex. The crystallographic 2-fold axis is indicated by a symbol at the center of the dimer. Disordered regions (residues 104–109 and 156–164) are shown by *dots*. The symmetry-related MAD2L2 and CAMP molecules are shown in *cyan* (safety belt: *light green*) and *pink*, respectively. *C*, secondary structures of MAD2L2. Secondary structure elements of Form-I and Form-II MAD2L2 are indicated *above and below the amino acid sequence*, respectively. Colors of secondary structure elements correspond to those in Fig. *A* or *B*. The β-strands are numbered in accordance with MAD2 structure (8). Disordered regions are indicated by *dashed lines*. *D*, comparison of the MAD2L2–CAMP and MAD2L2–REV3 complexes. Superimposition of the structures of MAD2L2–CAMP and MAD2L2–REV3 complexes is shown in the *upper panel*. Colors of the MAD2L2–CAMP complex correspond those in *A*. The MAD2L2–REV3 complex is shown in *silver* (MAD2L2) and *yellow* (REV3). A comparison of the amino acid sequences of CAMP and REV3 is shown in the *lower panel*. Trp-334 and Lys-335 in the WK motif of CAMP are shown in *magenta*. Secondary structure elements of CAMP and REV3 are indicated *above and below the amino acid sequences*. Disordered regions are indicated by *dashed lines*.

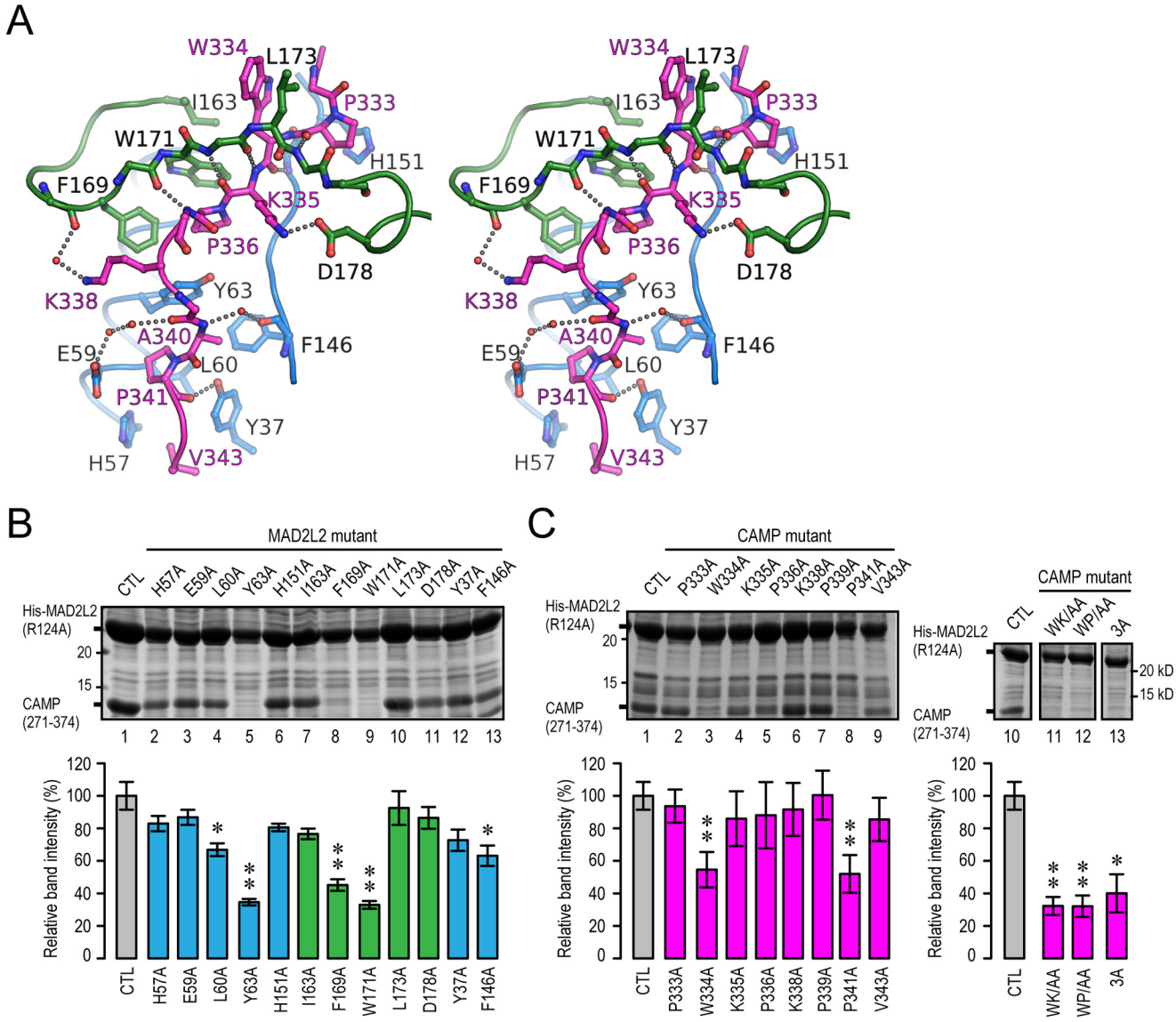

Figure 3. Interaction between MAD2L2 and the CAMP fragment. *A*, stereo view of the structural details of the interactions between MAD2L2 and CAMP. Colors correspond to those in Fig. 2*A*. Residues involved in the interaction are labeled. The orientation is same as the *right panel* in Fig. 2*A*. Water molecules are shown as *red spheres*. Electrostatic interactions are shown as *silver dots*. *B* and *C*, interaction analysis between MAD2L2 and the CAMP fragment. Results of SDS-PAGE are shown in the *upper panel*. *WA/KA* and *WA/PA* indicate W334A/K335A and W334A/P341A double mutants of CAMP, respectively. *3A* indicates W334A/K335A/P341A triple mutant of CAMP. Positions of molecular masses of 20 kDa and 15 kDa are indicated by *20* and *15*, respectively. The relative band intensities of CAMP divided by the band intensities of MAD2L2 were normalized to those of the control (*CTL*), and values are visualized as *bar graphs with standard error* (S.E.) *bars* ($n = 3$) in the *lower panel*. *Bar graphs* of controls are shown in *gray*. Other colors of bar graph correspond to those of Fig. 2*A*. The *asterisks* indicate statistically significant differences from control (Student's *t* test: *, $p < 0.05$; **, $p < 0.01$).

the MAD2L2–CAMP and MAD2L2–REV3 complexes adopt virtually the same structures.

Structural details of the interaction between MAD2L2 and CAMP

A previous structural study on the MAD2L2–REV3 complex revealed that multiple prolines of REV3 are crucially involved in the interaction with MAD2L2 (8). Pro-1880 of REV3 is accommodated in a pocket of MAD2L2, where the aromatic side chain of Trp-171 of MAD2L2 stacks with the ring of Pro-1880 of REV3. Both Pro-1884 and Pro-1885 of REV3 are accommodated in another pocket of MAD2L2, where the aromatic side chain of Tyr-63 of MAD2L2 also stacks with Pro-1884 of REV3, and van der Waals interactions surround Pro-1885 of REV3. The carbonyl oxygen of Pro-1885 is supported by a hydrogen bond formed with the side chain of Tyr-37 of MAD2L2. Consistent with the structural study, a biochemical study denoted the consensus sequence for MAD2L2-binding as $\phi\phi$XPXXXPP, where ϕ and X are a hydrophobic and any residue, respectively, and the second proline is less important than the third proline (25).

Distinct from REV3, the region from residues 325 to 344 of CAMP contains the sequence "PXXXAP," where the second proline is replaced with alanine (Fig. 2*D*). The present structure clarifies the mechanism of interaction between MAD2L2 and CAMP (Fig. 3*A*). Pro-336 of CAMP is accommodated in the pocket formed by Tyr-63, Phe-169, and Trp-171, where Pro-336 is recognized by Trp-171 of MAD2L2 via a stacking inter-

action, similar to the recognition of Pro-1880 of REV3. Ala-340 and Pro-341 are accommodated in the pocket formed by Tyr-37, Glu-59, Leu-60, Tyr-63, and Phe-146, also in a similar manner to Pro-1884 and Pro-1885 of REV3. The carbonyl oxygen of Pro-341 is also supported by a hydrogen bond formed with the side chain of Tyr-37 of MAD2L2, as observed for REV3. Although the CAMP fragment lacks the second proline, Tyr-63 of MAD2L2 still interacts with the corresponding residue, Ala-340, by van der Waals interactions. Interestingly, unlike the MAD2L2–REV3 complex, a water molecule is present in the pocket and forms hydrogen bonds with the amide nitrogen of Ala-340 of CAMP and the carbonyl oxygen of Phe-146 of MAD2L2, resulting in a network of hydrogen bonds. These interactions might compensate for the lack of stacking interactions that would be provided by the second proline (Pro-1884) of REV3. *Shigella* IpaB also interacts with MAD2L2 (26), and its binding region similarly contains alanine instead of the second proline, suggesting that a similar network with a water molecule might be involved in the interaction between MAD2L2 and IpaB. It seems, therefore, that the second proline is not necessary but can be replaced with a small residue such as alanine so that a water molecule can mediate the interaction.

The WK motif has been identified as a novel motif in CAMP (19). The crystal structure revealed that both Trp-334 and Lys-335 of the motif are involved in binding to MAD2L2 (Fig. 3*A*). The aromatic side chain of Trp-334 forms van der Waals interactions with Leu-173 of MAD2L2, and the basic side chain of Lys-335 interacts with the acidic side chain of Asp-178 of MAD2L2 via ionic contacts. Furthermore, the ring of Pro-333 preceding the WK residues stacks with the aromatic side chain of His-151 of MAD2L2. In addition to the interactions described above, hydrogen bonds mediated by water molecules are involved in the interaction between MAD2L2 and CAMP (Fig. 3*A*).

Analysis of the MAD2L2–CAMP interaction

To pinpoint the significant interactions in the MAD2L2–CAMP complex, residues of CAMP or MAD2L2 were replaced with alanine, and the amount of CAMP fragment that co-purified with immobilized His-tagged MAD2L2 was evaluated (Fig. 3, *B* and *C*). As expected, mutation of Tyr-63 or Trp-171 in MAD2L2 markedly reduced the interaction between MAD2L2 and CAMP (*lane 5* or *9* in Fig. 3*B*), as did mutation of Phe-169 (*lane 8* in Fig. 3*B*), suggesting that van der Waals interactions formed by these aromatic residues of MAD2L2 are crucial for formation of the MAD2L2–CAMP complex (Fig. 3*A*). In contrast, mutation of Pro-336 in CAMP only slightly impaired the interaction between MAD2L2 and CAMP (*lane 5* in Fig. 3*C*), although mutation of Pro-341 in CAMP had a large impact on the interaction, as expected (*lane 8* in Fig. 3*C*). This indicates that the stacking interaction between Trp-171 of MAD2L2 and Pro-336 of CAMP is less important for formation of the MAD2L2–CAMP complex, in contrast to the significant contribution of the stacking interaction between Trp-171 and Pro-1880 in formation of the MAD2L2–REV3 complex (8, 25).

More interestingly, mutation of Trp-334 in the WK motif of CAMP greatly reduced the interaction (*lane 3* in Fig. 3*C*), whereas mutation of Lys-335 had only a small impact (*lane 4* in Fig. 3*C*). Furthermore, double (W334A/K335A, W334A/P341A) and triple (W334A/P336A/P341A) mutations markedly reduced the interaction (*lane 11*, *12*, or *13* in Fig. 3*C*). These results suggest that the formation mechanism of the MAD2L2–CAMP complex differs from that of the MAD2L2–REV3 complex; namely, van der Waals interactions provided by Trp-334 and Pro-341 of CAMP are mainly responsible for the interaction with MAD2L2, whereas Pro-333, Lys-335, and Pro-336 make a moderate contribution that might be utilized for fine-tuning to increase the specificity of the interaction between MAD2L2 and CAMP. As described above, the P336A mutation in CAMP had a small effect on the interaction with MAD2L2, although the W171A mutation in MAD2L2 led to a marked reduction of binding affinity. This suggests that van der Waals interactions made by Ala-336 in CAMP mutant might be sufficient to form the MAD2L2–CAMP complex due to a large contribution from residues such as Trp-334 and Pro-341 and/or a supportive contribution from other residues.

To verify the results of the *in vitro* interaction between MAD2L2 and CAMP in human cells, immunoprecipitation assays using full-length CAMP were performed (Fig. 4). In good agreement with the *in vitro* results, Y63A, W171A, and Y63A/W171A mutations of MAD2L2 had a substantial impact on the interaction with CAMP (Fig. 4, *A* and *B*). Furthermore, the W334A/K335A, W334A/P341A, and W334A/K335A/P341A mutations of CAMP abolished the interaction with MAD2L2 (Fig. 4, *C* and *D*). Significantly, the deletion of residues 324–350 in CAMP also abolished the interaction (Fig. 4, *C* and *D*). These observations indicate that the structure and interaction of the MAD2L2–CAMP complex described here is likely to reflect those in human cells. Consistently, mutations in MAD2L2 had an impact on the localization of MAD2L2 in mitotic cells (Fig. 5). Wild-type MAD2L2 was co-localized with full-length CAMP in the mitotic spindle and mitotic chromosomes (Fig. 5*A*). Wild-type MAD2L2 was localized to the mitotic spindle and to mitotic chromosomes, whereas MAD2L2 carrying the Y63A, W171A, or Y63A/W171A mutation was not detected in mitotic chromosomes (Fig. 5*B*). This clearly indicates that the interactions observed in the crystal structure are essential for co-localization with CAMP at chromosomes in mitotic cells. Interestingly, MAD2L2 carrying these mutations could still localize to the mitotic spindle. This implies that MAD2L2 may have mitotic partners other than CAMP and might interact with those proteins by alternative mechanisms. Previous studies have shown that MAD2L2 interacts with spindle-related proteins such as the small GTPase RAN (17) and clathrin light chain A (CLTA) (27). MAD2L2 might retain localization in spindle by interactions with such spindle-related proteins. Further analyses will be required to explain localization of MAD2L2 in mitotic spindles. Taken together with the crystal structure and interaction assay results, these findings reveal the interaction mechanism distinct from that of MAD2L2–REV3 complex.

The structure-based interaction analysis by IMAC revealed that Trp-334 and Pro-341 of CAMP were most crucial for the binding to MAD2L2. Among 13 WK sequences of CAMP, WK-4, -7, and -8, have both corresponding tryptophan and proline residues. WK-7 and -8 have SP instead of ^{340}AP^{341} in WK-4, implying that the polar side chain of the serine residue would be unsuitable to contact Phe-146 (Fig. 3*A*). In addition,

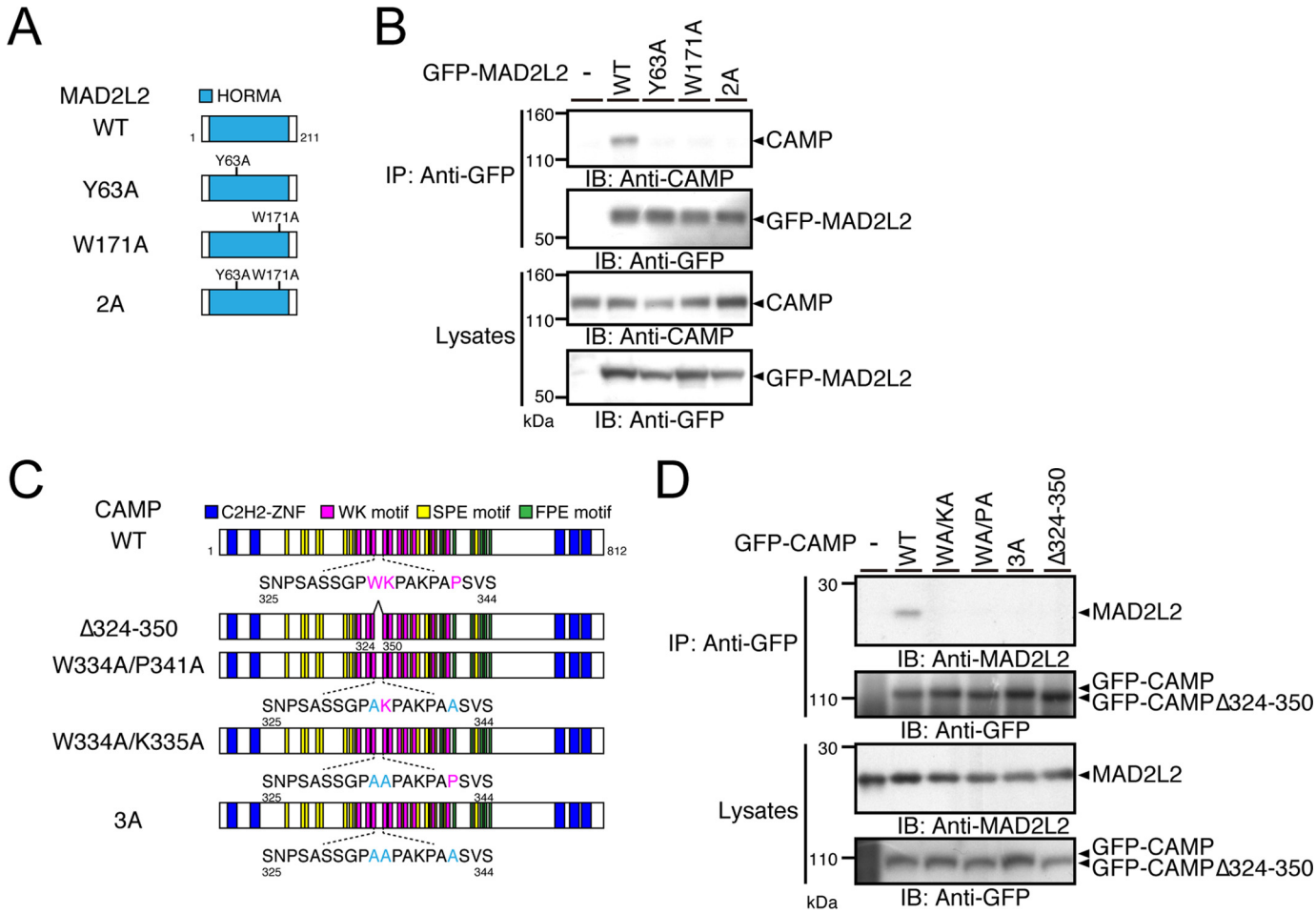

Figure 4. Analysis of the interaction between CAMP and MAD2L2 by immunoprecipitation. *A*, schematic representation of the MAD2L2 mutants used in this study. Location of the HORMA domain and the amino acid residues likely to be responsible for CAMP-binding are shown. *B*, cell lysates were immunoprecipitated with anti-GFP antibody. Precipitates were separated by SDS-PAGE and analyzed by Western blotting using the indicated antibodies. *C*, schematic diagram of the CAMP mutants used in this study. The location of the C2H2-Zn finger domain, multiple repeat motifs (WK, SPE, FPE) and the position of the amino acid residues likely to be involved in MAD2L2 binding are shown. *WA/KA* and *WA/PA* indicate W334A/K335A and W334A/P341A double mutants, respectively. *3A* indicates W334A/K335A/P341A triple mutant of CAMP. *D*, cell lysates expressing GFP-CAMP mutants were subjected to immunoprecipitation and analyzed by Western blotting using antibodies specific for MAD2L2 and GFP.

WK-7 and -8 lack the proline residue preceding WK. These observations suggest that WK-4 could be determinant to interact with MAD2L2. In fact, co-immunoprecipitation assays revealed that the deletion of residues 324–350 in CAMP, the lacking WK-4 and WK-5, abolished the interaction with MAD2L2 (Fig. 4*D*). WK-5 lacks AP and has ^{354}VS^{355} instead, suggesting that WK-5 is unlikely involved in the interaction with MAD2L2. Therefore, we conclude that the CAMP fragment including WK-4 is responsible for the MAD2L2 interaction.

Dynamic feature of the C-terminal region of MAD2L2

In the Form-II crystal, the MAD2L2–CAMP complex forms a dimeric structure in which the C-terminal region of MAD2L2 is swapped between the dimers (Fig. 2*B*). The secondary structures of the swapped region are rearranged as follows (Fig. 2, *B* and *C*). The β8′ strand, which interacts with the swapped β8′′ from another complex is shortened. The following β8′′ strand is extended to the other complex and interacts with β8′ and β5, thereby forming a β-sheet structure (Fig. 2*B*). Furthermore, the αE helix is newly formed between β8′ and β8′′, whereas the αD helix is loosened, and the N-terminal portion of αC is pushed away by the αE; thus, the structure of the region β5-αC is altered (Figs. 2, *B* and *D*, and 6), consistent with our observation of flexible features relative to the structure of the MAD2–REV3 complex (Fig. 2*D*).

To avoid steric hindrance from αC, the side chain of Phe-126 is flipped (Fig. 6). More interestingly, the swapped β8′′ strand of the Form-II structure is shifted by two residues relative to the Form-I structure, thereby fastening of the safety belt is incomplete (Fig. 6). Namely, the C-terminal region adopts an immature structure. In more detail, three hydrophobic residues, Leu-197, Met-199, and Leu-201, of the Form-II structure are nicely in line with, respectively, Met-199, Leu-201, and Val-203 of the Form-I structure. Given these observations, the structure of the C-terminal region of MAD2L2 is inherently flexible, and the plasticity may be correlated with the mechanism of complex formation or the function of MAD2L2.

Discussion

The crystal structure of MAD2L2 in complex with a CAMP fragment was determined in two forms, Form-I and Form-II. The Form-I structure revealed that MAD2L2 binds to CAMP via its C-terminal region termed the safety belt as also observed

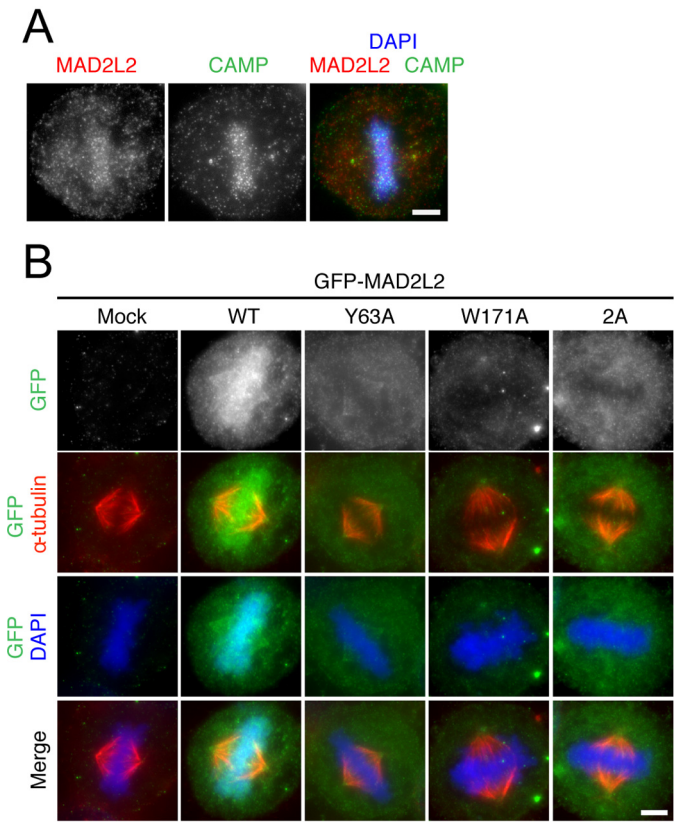

Figure 5. Localization analysis of MAD2L2 by immunofluorescence. *A*, co-localization of MAD2L2 and CAMP. HeLa Kyoto cells released from thymidine block for 10 h were fixed and stained with antibodies against MAD2L2 (*red*) and CAMP (*green*). DNA was stained with DAPI (*blue*). *Scale bar*: 5 μm. *B*, HeLa Kyoto cells expressing GFP-MAD2L2 constructs were released from thymidine block for 10 h, fixed, and stained with antibodies to GFP (*green*) and α-tubulin (*red*). DNA was probed with DAPI (*blue*). *Scale bar*: 5 μm. 2*A* indicates Y63A/W171A double mutant of MAD2L2.

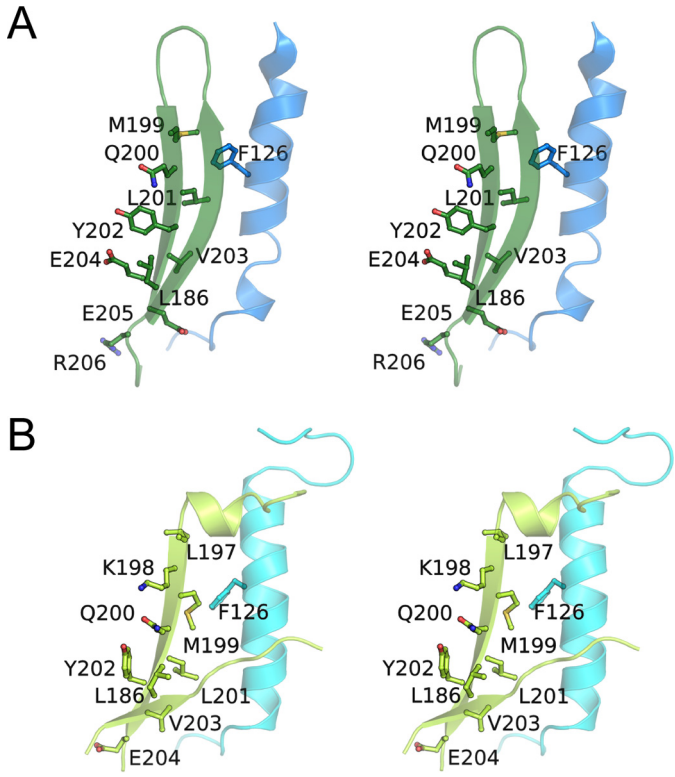

Figure 6. Comparison of the Form-I and Form-II structures. *A* and *B*, stereo view of the detailed structures of the Form-I (*A*) and Form-II (*B*) C-terminal regions, shown in overlaid orientation. Residues discussed in this work are labeled. For clarification, ribbon models are shown in transparent representation.

in the MAD2L2–REV3 complex (8). However, the mechanism underlying formation of the complex differs from that of the REV3 complex. Namely, the importance of the contribution made by each interaction varies between the two complexes; these differences might be the result of fine-turning interactions that have evolved to increase the specificity for partner proteins. Such a strategy would be reasonable for the maintenance of PPI networks connected to a hub protein, because it might reduce the impact on cellular functions caused by blocking a certain PPI by mutations or inhibitors. In other words, a structural basis for the diverse mechanisms of interaction between MAD2L2 and partner proteins might facilitate the development of specific inhibitors for MAD2L2-related PPIs.

The Form-II structure revealed the dynamic feature of the C-terminal region of MAD2L2. This could have an analogy with the spindle assembly checkpoint protein, MAD2. In humans, MAD2 shares 22% amino acid identity with MAD2L2, which on interaction with its partner proteins undergoes a marked conformational change from an open (O-MAD2) to a closed (C-MAD2) conformer whereby the C-terminal region of MAD2 moves from the edge of the β6 sheet toward the edge of the β5 sheet to bind the target (24, 28). A previous study based on circular dichroism spectra suggested that MAD2L2 also undergoes a conformational change in its C-terminal region to bind REV3 (29). Although the structure of MAD2L2 without a partner protein, namely the "open" structure of MAD2L2, remains unknown, the present study provides convincing data to support a mechanism in which the C-terminal region of MAD2L2 opens and closes to bind a partner protein. Energetic studies have clarified that MAD2 functions in checkpoint activation via the formation of several types of dimer through the αC helix (30–34), whereas whether MAD2L2 functions as a dimer is an open question. Recently, a second MAD2L2-binding site was identified in REV3, implying that the dimeric feature of MAD2L2 might facilitate two-site binding to REV3 to increase affinity and specificity or dimer formation might promote simultaneous interactions with multiple proteins (35). The size exclusion chromatography purification for the MAD2L2–CAMP complex used in this crystallographic study shows that the complex exists as a monomer in solution; thus, the swapped dimer in the Form-II may be an artifact in crystallization. Alternatively, the Form-II structure implies that formation of the incompletely fastened safety belt may be possible in the monomeric complex, and the immature structure might reflect an intermediate state during the partner binding. Arrangement of amino acid residues on the β8′ and β8′′ strands, namely the second PPI face, are altered (Fig. 6). REV1 binds to the β8′ and β8′′ strands of MAD2L2, and Leu-186, Gln-200, and Tyr-202 on these strands are crucial for the interaction. In the incompletely fastened safety belt, Leu-186 is located in a position similar to that in the Form-I structure or previous structures of MAD2L2 complexes, whereas Gln-200 and Tyr-202 on the β8′′ strand have shifted positions (Fig. 6), supposedly impairing

REV1 binding. Thus, the immature structure of the safety belt would prevent the second PPI. In other words, the structure of safety belt may regulate the availability of the second PPI. This implication is consistent with the PPI model of MAD2L2 (8, 10). The biological and functional relevance of the incompletely fastened safety belt and dimer formation of MAD2L2 are puzzles to be solved by further study.

In summary, we have presented the structure of MAD2L2 in complex with a CAMP fragment, thereby revealing the structural basis of the interaction between MAD2L2 and CAMP. This work is the first structural study to examine a MAD2L2 interaction not involved in TLS, and it might pave the way to clarifying the mitotic roles of MAD2L2. Furthermore, we have revealed new structural features of MAD2L2, providing mechanistic implications of PPIs by MAD2L2. Recently, biological functions of MAD2L2 in non-homologous end-joining and DNA cross-link repair have been rediscovered (36–38). Therefore, it is becoming increasing crucial to clarify the mechanisms of PPIs engaged by MAD2L2, and these are our future goals.

Experimental procedures

Protein production and purification

The central region of human CAMP including the WK motifs (residues 271–490) is known to interact with MAD2L2 (19). To optimize the MAD2L2-interacting region for the present crystallographic study, a series of co-expression vectors derived from the pET-Duet1 vector (Novagen) and containing cDNAs of human His-tagged MAD2L2 and a human CAMP fragment varying in length from residues 271 to residues 490 were constructed and evaluated for protein production, purification, and crystallization. Consequently, MAD2L2 in complex with a CAMP fragment comprising residues 325–344 was successfully crystallized. Protein production and purification of this MADL2L2–CAMP complex are described in detail below.

The cDNA encoding human CAMP (residues 325–344) was cloned into the NdeI-XhoI site of pET-Duet1 containing the cDNA of human MAD2L2 in the EcoRI-PstI site (29), producing a vector expressing Mad2L2 with an N-terminal hexameric histidine tag and the CAMP fragment. In this study an R124A mutation was introduced in MAD2L2 to facilitate crystallization (8, 29). The expression vector was used to transform *Escherichia coli* BL21(DE3)CodonPlus. Cells were grown at 310 K to a cell density of ~1.0 at 660 nm in LB medium and then cultured for a further ~20 h at 288 K after the addition of 0.2 mM isopropyl β-D-1-thiogalactopyranoside. The harvested cells were suspended in 10 ml of buffer I (50 mM HEPES-NaOH, pH 7.4, and 500 mM NaCl) per gram of cells and lysed by sonication. The cell lysate was clarified by centrifugation for 1 h at 277 K (48,300 × *g*). Subsequent purification was carried out at 277 K. The supernatant was applied to a nickel-nitrilotriacetic acid-agarose resin (Qiagen), and the resin was washed first with buffer II (50 mM HEPES-NaOH, pH 7.4, and 1.5 M NaCl) and then with buffer III (50 mM HEPES-NaOH, pH 7.4, and 100 mM NaCl). The His-tagged MAD2L2–CAMP complex was eluted stepwise with buffer III containing 50–500 mM imidazole, diluted with buffer IV (50 mM Tris-HCl, pH 8.5), and then applied to an anion-exchange column, HiTrap Q HP (5 ml) (GE Healthcare). The bound protein was eluted with a linear gradient of 0 to 500 mM NaCl over a total volume of 95 ml. The eluted protein passed through a size exclusion column, HiLoad 16/600 Superdex 75 pg (GE Healthcare), equilibrated with buffer V (20 mM HEPES-NaOH, pH 7.4, and 100 mM NaCl) and then concentrated to 20 mg/ml using a Vivaspin (10-kDa nominal molecular weight limit) concentrator (Sartorius). The purity of the MAD2L2–CAMP complex was confirmed by SDS-PAGE with Coomassie Brilliant Blue staining. The purified protein was frozen with liquid N_2 and stored at 193 K until use.

Crystallization, data collection, and structure determination

Crystallization of the MAD2L2–CAMP complex was performed by the sitting drop vapor-diffusion method using a commercial kit to screen crystallization conditions. Drops were prepared by mixing 0.5 μl of protein solution with 0.5 μl of reservoir solution. Crystals were obtained under several conditions after a week at 293 K. After optimization of the conditions, crystals suitable for X-ray diffraction study were eventually grown in two crystal forms: Form-I and Form-II. Crystals of Form-I were obtained with a reservoir solution consisting of 0.1 M sodium cacodylate, pH 6.6, and 4.0 M sodium formate. Crystals of Form-II were obtained with a reservoir solution consisting of 0.3 M potassium thiocyanate and 20% PEG 3350.

Before the X-ray diffraction study, the crystals were transferred to a buffer comprising the reservoir solution plus 20% ethylene glycol for cryo-protection. Each crystal was picked up in a nylon loop and cooled and stored in liquid N_2 via an Universal V1-Puck (Crystal Positioning System, Inc.) until use. X-ray diffraction data of frozen crystals were collected under a stream of N_2 gas at 100 K on the BL-17A beamline at Photon Factory (Tsukuba, Japan) using a pixel array photon-counting detector, PILATUS3 S6M (DECTRIS). Diffraction data were integrated, scaled, and averaged with programs *XDS* (39) and *SCALA* (40).

The crystal structures of the MAD2L2–CAMP complex were determined by molecular replacement using the structure of REV7–REV3 complex (PDB ID 3ABD) as a search model with the program *PHASER* (41). Manual model building and fitting were performed by the program COOT (42) followed by structure refinement using the program *PHENIX* (43). Structure factors and final coordinates were deposited in the Protein Data Bank (PDB IDs 5XPT and 5XPU). The data collection and refinement statistics are given in Table 1. Secondary structures are defined with the program *DSSP* (44).

Interaction analysis by bacterial co-expression and IMAC

A cDNA encoding a human CAMP fragment (residues 271–374) was cloned into the NdeI-XhoI site of pET-Duet1 containing the cDNA of human MAD2L2 in the EcoRI-PstI site (29). Site-directed mutations in MAD2L2 or CAMP were introduced by using a PCR-based method. His-tagged MAD2L2 was co-expressed with the CAMP fragment by a procedure similar to that described above. Interaction analysis by IMAC was performed as described previously (8). In brief, the cell lysate was applied to nickel-Sepharose High Performance beads (GE Healthcare). The beads were washed first with buffer II and then with buffer III. The bound proteins were analyzed by SDS-PAGE with Coomassie Brilliant Blue staining and the

Table 1
Data collection and refinement statistics
Values in parentheses are those for the high resolution range.

Statistics	Form-I	Form-II
Data collection		
Wavelength (Å)	0.98000	0.98000
Space group	*I* 422	*C* 2
a (Å)	106.5	71.03
b (Å)	106.5	70.56
c (Å)	127.4	45.13
β (°)	90	90.29
Resolution (Å)	19.85-2.10 (2.18-2.10)	19.09-2.30 (2.39-2.30)
Observed reflections	282,735 (27,574)	33,668 (3,337)
Unique reflections	21,579 (2,071)	9,883 (982)
Multiplicity	13.1 (13.3)	3.4 (3.4)
R-merge	0.081 (0.727)	0.058 (0.637)
Completeness (%)	99.8 (97.6)	99.6 (98.0)
$\langle I \rangle / \sigma \langle I \rangle$	27.5 (3.5)	13.5 (2.1)
Mosaicity	0.14	0.19
Refinement		
Resolution (Å)	19.85-2.10	19.09-2.30
Refined reflections	21,575	9,876
Free reflections	1,063	479
R-work	0.197	0.219
R-free	0.226	0.227
Root mean square deviation		
Bond lengths (Å)	0.008	0.010
Bond angles (°)	1.110	1.269
Protein Data Bank ID	5XPT	5XPU

ChemiDoc Touch Imaging System (Bio-Rad). These assays were performed three times.

Interaction analysis by immunoprecipitation

The cDNA for human CAMP was cloned as described previously (19). The cDNA for human MAD2L2 was amplified by PCR from the MegaMan human transcriptome cDNA library (Agilent Technologies). The cDNAs for CAMP-truncated mutants were created by PCR. These cDNAs were subcloned into pEGFP-C1 (Clontech). The cDNAs for point mutation of CAMP and MAD2L2 were generated by using the QuikChange site-directed mutagenesis kit (Stratagene) according to the manufacturer's instructions.

HeLa Kyoto cells were cultured in Dulbecco's modified Eagle's medium (DMEM) supplemented with 10% fetal bovine serum. Transfection of GFP-tagged CAMP or MAD2L2 constructs was performed by using FuGENE HD Transfection reagent (Promega) according to the manufacturer's instructions. For synchronization at early mitotic phase, HeLa Kyoto cells transfected with GFP-tagged MAD2L2 mutants were incubated for 12 h and then cultured in the presence of 2 mM thymidine for 24 h, released from thymidine block for 10 h, and fixed and stained.

The following rabbit polyclonal antibodies were used in immunofluorescence (IF), Western blotting (WB), and immunoprecipitation (IP): anti-CAMP (Sigma, HPA008900) diluted at 1:500 for IF and WB, and anti-GFP (Life Technologies, A11122) diluted at 1:1000 for WB and IP. The mouse monoclonal antibody against MAD2L2 (BD Transduction Laboratories, 612266) was used at a dilution of 1:500 for WB and at a dilution of 1:250 for IF.

HeLa Kyoto cells expressing GFP-tagged CAMP or MAD2L2 constructs were lysed and sonicated in lysis buffer (20 mM Tris-HCl, pH 7.5, 150 mM NaCl, 1% Nonidet P-40, 10% glycerol, 0.5 mM EGTA, and 1 mM DTT) supplemented with phosphatase inhibitor mixture (Roche Applied Science) and protease inhibitor mixture (Roche Applied Science). After centrifugation for 10 min at 277 K at 16,000 × *g*, the supernatants were precleared with IgG-conjugated magnetic beads (Dynabeads M-280, ThermoFisher Scientific) for 1 h at 277 K and incubated with antibody against GFP for 1 h at 277 K and then with IgG-conjugated magnetic beads for 2 h at 277 K. Precipitates were washed three times with lysis buffer, and the samples were then separated by SDS-PAGE and analyzed by immunoblotting.

Immunofluorescence and microscopy

Cells were fixed with ice-cold methanol for 10 min at 253 K after pre-extraction using PHEM buffer pH 7.0 containing 60 mM PIPES, 25 mM HEPES, 10 mM EGTA, 2 mM $MgSO_4$, and 0.1% Triton X-100 for 1 min at room temperature, blocked with phosphate-buffer saline containing 3% BSA and 0.01% Triton X-100 at room temperature for 30 min, and then incubated with primary antibodies overnight at 277 K. Goat anti-rabbit IgG Alexa-Fluor 488 and goat anti-mouse Alexa-Fluor 568 (Molecular Probes) were used as secondary antibodies. Immunofluorescence images were obtained using a Personal DV microscope (Applied Precision) equipped with a Plan Apochromat 100× oil objective lens (NA 1.40) (Olympus) mounted on an inverted microscope (CoolSNAP HQ; Photometrics), driven by softWoRx software (Applied Precision, LLC).

Figure presentation

Figures of protein structures were prepared with the program PyMOL (Schrödinger, LLC). All of figures were modified with the program *Illustrator* (Adobe Systems).

Author contributions—K. H. and S. T. designed the experiments and carried out protein production, crystallization, structure determination, and the *in vitro* interaction assay. M. I., H. F., Y. M., S.-i. K., and K. T. performed the immunoprecipitation and immunofluorescence analyses. K. H. and H. H. drafted the manuscript. S. K., A. H., H. Y., and Y. I. discussed and interpreted the experimental data. All authors revised and agreed to the final version of the manuscript.

Acknowledgment—We acknowledge the kind support of the beamline staff of PF for data collection.

References

1. Lawrence, C. W., Das, G., and Christensen, R. B. (1985) REV7, a new gene concerned with UV mutagenesis in yeast. *Mol. Gen. Genet.* **200,** 80–85
2. Lawrence, C. W., Nisson, P. E., and Christensen, R. B. (1985) UV and chemical mutagenesis in *rev7* mutants of yeast. *Mol. Gen. Genet.* **200,** 86–91
3. Torpey, L. E., Gibbs, P. E., Nelson, J., and Lawrence, C. W. (1994) Cloning and sequence of *REV7*, a gene whose function is required for DNA damage-induced mutagenesis in *Saccharomyces cerevisiae*. *Yeast* **10,** 1503–1509
4. Nelson, J. R., Lawrence, C. W., and Hinkle, D. C. (1996) Thymine-thymine dimer bypass by yeast DNA polymerase ζ. *Science* **272,** 1646–1649
5. Murakumo, Y., Roth, T., Ishii, H., Rasio, D., Numata, S., Croce, C. M., and Fishel, R. (2000) A human REV7 homolog that interacts with the polymerase ζ catalytic subunit hREV3 and the spindle assembly checkpoint protein hMAD2. *J. Biol. Chem.* **275,** 4391–4397
6. Murakumo, Y., Ogura, Y., Ishii, H., Numata, S., Ichihara, M., Croce, C. M., Fishel, R., and Takahashi, M. (2001) Interactions in the error-prone postreplication repair proteins hREV1, hREV3, and hREV7. *J. Biol. Chem.* **276,** 35644–35651
7. Masuda, Y., Ohmae, M., Masuda, K., and Kamiya, K. (2003) Structure and enzymatic properties of a stable complex of the human REV1 and REV7 proteins. *J. Biol. Chem.* **278,** 12356–12360

8. Hara, K., Hashimoto, H., Murakumo, Y., Kobayashi, S., Kogame, T., Unzai, S., Akashi, S., Takeda, S., Shimizu, T., and Sato, M. (2010) Crystal structure of human REV7 in complex with a human REV3 fragment and structural implication of the interaction between DNA polymerase ζ and REV1. *J. Biol. Chem.* **285,** 12299–12307
9. Wojtaszek, J., Lee, C. J., D'Souza, S., Minesinger, B., Kim, H., D'Andrea, A. D., Walker, G. C., and Zhou, P. (2012) Structural basis of Rev1-mediated assembly of a quaternary vertebrate translesion polymerase complex consisting of Rev1, heterodimeric polymerase (Pol) ζ, and Pol κ. *J. Biol. Chem.* **287,** 33836–33846
10. Kikuchi, S., Hara, K., Shimizu, T., Sato, M., and Hashimoto, H. (2012) Structural basis of recruitment of DNA polymerase ζ by interaction between REV1 and REV7 proteins. *J. Biol. Chem.* **287,** 33847–33852
11. Xie, W., Yang, X., Xu, M., and Jiang, T. (2012) Structural insights into the assembly of human translesion polymerase complexes. *Protein Cell* **3,** 864–874
12. Liu, D., Ryu, K. S., Ko, J., Sun, D., Lim, K., Lee, J. O., Hwang, J. m., Lee, Z. W., and Choi, B. S. (2013) Insights into the regulation of human Rev1 for translesion synthesis polymerases revealed by the structural studies on its polymerase-interacting domain. *J. Mol. Cell. Biol.* **5,** 204–206
13. Pfleger, C. M., Salic, A., Lee, E., and Kirschner, M. W. (2001) Inhibition of Cdh1-APC by the MAD2-related protein MAD2L2: a novel mechanism for regulating Cdh1. *Genes Dev.* **15,** 1759–1764
14. Chen, J., and Fang, G. (2001) MAD2B is an inhibitor of the anaphase-promoting complex. *Genes Dev.* **15,** 1765–1770
15. Listovsky, T., and Sale, J. E. (2013) Sequestration of CDH1 by MAD2L2 prevents premature APC/C activation prior to anaphase onset. *J. Cell Biol.* **203,** 87–100
16. Bhat, A., Wu, Z., Maher, V. M., McCormick, J. J., and Xiao, W. (2015) Rev7/Mad2B plays a critical role in the assembly of a functional mitotic spindle. *Cell Cycle* **14,** 3929–3938
17. Medendorp, K., van Groningen, J. J., Vreede, L., Hetterschijt, L., van den Hurk, W. H., de Bruijn, D. R., Brugmans, L., and van Kessel, A. G. (2009) The mitotic arrest deficient protein MAD2B interacts with the small GTPase RAN throughout the cell cycle. *PLoS ONE* **4,** e7020
18. Vermeulen, M., Eberl, H. C., Matarese, F., Marks, H., Denissov, S., Butter, F., Lee, K. K., Olsen, J. V., Hyman, A. A., Stunnenberg, H. G., and Mann, M. (2010) Quantitative interaction proteomics and genome-wide profiling of epigenetic histone marks and their readers. *Cell* **142,** 967–980
19. Itoh, G., Kanno, S., Uchida, K. S., Chiba, S., Sugino, S., Watanabe, K., Mizuno, K., Yasui, A., Hirota, T., and Tanaka, K. (2011) CAMP (C13orf8, ZNF828) is a novel regulator of kinetochore-microtubule attachment. *EMBO J.* **30,** 130–144
20. Deciphering Developmental Disorders Study (2015) Large-scale discovery of novel genetic causes of developmental disorders. *Nature* **519,** 223–228
21. Hempel, M., Cremer, K., Ockeloen, C. W., Lichtenbelt, K. D., Herkert, J. C., Denecke, J., Haack, T. B., Zink, A. M., Becker, J., Wohlleber, E., Johannsen, J., Alhaddad, B., Pfundt, R., Fuchs, S., Wieczorek, D., Strom, T. M., *et al.* (2015) *De novo* mutations in CHAMP1 cause intellectual disability with severe speech impairment. *Am. J. Hum. Genet.* **97,** 493–500
22. Tanaka, A. J., Cho, M. T., Retterer, K., Jones, J. R., Nowak, C., Douglas, J., Jiang, Y. H., McConkie-Rosell, A., Schaefer, G. B., Kaylor, J., Rahman, O. A., Telegrafi, A., Friedman, B., Douglas, G., Monaghan, K. G., and Chung, W. K. (2016) *De novo* pathogenic variants in CHAMP1 are associated with global developmental delay, intellectual disability, and dysmorphic facial features. *Cold Spring Harb. Mol. Case. Stud.* **2,** a000661
23. Isidor, B., Küry, S., Rosenfeld, J. A., Besnard, T., Schmitt, S., Joss, S., Davies, S. J., Lebel, R. R., Henderson, A., Schaaf, C. P., Streff, H. E., Yang, Y., Jain, V., Chida, N., Latypova, X., Le Caignec, C., Cogné, B., *et al.* (2016) *De Novo* truncating mutations in the kinetochore-microtubules attachment gene CHAMP1 cause syndromic intellectual disability. *Hum. Mutat.* **37,** 354–358
24. Sironi, L., Mapelli, M., Knapp, S., De Antoni, A., Jeang, K. T., and Musacchio, A. (2002) Crystal structure of the tetrameric Mad1-Mad2 core complex: implications of a "safety belt" binding mechanism for the spindle checkpoint. *EMBO J.* **21,** 2496–2506
25. Hanafusa, T., Habu, T., Tomida, J., Ohashi, E., Murakumo, Y., and Ohmori, H. (2010) Overlapping in short motif sequences for binding to human REV7 and MAD2 proteins. *Genes Cells* **15,** 281–296
26. Iwai, H., Kim, M., Yoshikawa, Y., Ashida, H., Ogawa, M., Fujita, Y., Muller, D., Kirikae, T., Jackson, P. K., Kotani, S., and Sasakawa, C. (2007) A bacterial effector targets Mad2L2, an APC inhibitor, to modulate host cell cycling. *Cell* **130,** 611–623
27. Medendorp, K., Vreede, L., van Groningen, J. J., Hetterschijt, L., Brugmans, L., Jansen, P. A., van den Hurk, W. H., de Bruijn, D. R., and van Kessel, A. G. (2010) The mitotic arrest deficient protein MAD2B interacts with the clathrin light chain A during mitosis. *PLoS ONE* **5,** e15128
28. Luo, X., Tang, Z., Rizo, J., and Yu, H. (2002) The Mad2 spindle checkpoint protein undergoes similar major conformational changes upon binding to either Mad1 or Cdc20. *Mol. Cell* **9,** 59–71
29. Hara, K., Shimizu, T., Unzai, S., Akashi, S., Sato, M., and Hashimoto, H. (2009) Purification, crystallization, and initial X-ray diffraction study of human REV7 in complex with a REV3 fragment. *Acta Crystallogr. Sect. F Struct. Biol. Cryst. Commun.* **65,** 1302–1305
30. Yang, M., Li, B., Tomchick, D. R., Machius, M., Rizo, J., Yu, H., and Luo, X. (2007) $p31^{comet}$ blocks Mad2 activation through structural mimicry. *Cell* **131,** 744–755
31. Mapelli, M., Massimiliano, L., Santaguida, S., and Musacchio, A. (2007) The Mad2 conformational dimer: structure and implications for the spindle assembly checkpoint. *Cell* **131,** 730–743
32. Yang, M., Li, B., Liu, C. J., Tomchick, D. R., Machius, M., Rizo, J., Yu, H., and Luo, X. (2008) Insights into mad2 regulation in the spindle checkpoint revealed by the crystal structure of the symmetric mad2 dimer. *PLoS Biol.* **6,** e50
33. Hara, M., Özkan, E., Sun, H., Yu, H., and Luo, X. (2015) Structure of an intermediate conformer of the spindle checkpoint protein Mad2. *Proc. Natl. Acad. Sci. U.S.A.* **112,** 11252–11257
34. Luo, X., and Yu, H. (2008) Protein metamorphosis: the two-state behavior of Mad2. *Structure* **16,** 1616–1625
35. Tomida, J., Takata, K., Lange, S. S., Schibler, A. C., Yousefzadeh, M. J., Bhetawal, S., Dent, S. Y., and Wood, R. D. (2015) REV7 is essential for DNA damage tolerance via two REV3L binding sites in mammalian DNA polymerase ζ. *Nucleic Acids Res.* **43,** 1000–1011
36. Boersma, V., Moatti, N., Segura-Bayona, S., Peuscher, M. H., van der Torre, J., Wevers, B. A., Orthwein, A., Durocher, D., and Jacobs, J. J. L. (2015) MAD2L2 controls DNA repair at telomeres and DNA breaks by inhibiting 5′ end resection. *Nature* **521,** 537–540
37. Xu, G., Chapman, J. R., Brandsma, I., Yuan, J., Mistrik, M., Bouwman, P., Bartkova, J., Gogola, E., Warmerdam, D., Barazas, M., Jaspers, J. E., Watanabe, K., Pieterse, M., Kersbergen, A., Sol, W., *et al.* (2015) REV7 counteracts DNA double-strand break resection and affects PARP inhibition. *Nature* **521,** 541–544
38. Bluteau, D., Masliah-Planchon, J., Clairmont, C., Rousseau, A., Ceccaldi, R., Dubois d'Enghien, C., Bluteau, O., Cuccuini, W., Gachet, S., Peffault de Latour, R., Leblanc, T., Socié, G., Baruchel, A., Stoppa-Lyonnet, D., D'Andrea, A. D., and Soulier, J. (2016) Biallelic inactivation of *REV7* is associated with Fanconi anemia. *J. Clin. Invest.* **126,** 3580–3584
39. Kabsch, W. (2010) XDS. *Acta Crystallogr. D.* **66,** 125–132
40. Evans, P. (2006) Scaling and assessment of data quality. *Acta Crystallogr. D.* **62,** 72–82
41. McCoy, A. J., Grosse-Kunstleve, R. W., Adams, P. D., Winn, M. D., Storoni, L. C., and Read, R. J. (2007) Phaser crystallographic software. *J. Appl. Crystallogr.* **40,** 658–674
42. Emsley, P., and Cowtan, K. (2004) Coot: model-building tools for molecular graphics. *Acta Crystallogr. D.* **60,** 2126–2132
43. Adams, P. D., Afonine, P. V., Bunkóczi, G., Chen, V. B., Davis, I. W., Echols, N., Headd, J. J., Hung, L. W., Kapral, G. J., Grosse-Kunstleve, R. W., McCoy, A. J., Moriarty, N. W., Oeffner, R., Read, R. J., Richardson, D. C., Richardson, J. S., Terwilliger, T. C., and Zwart, P. H. (2010) *PHENIX*: a comprehensive Python-based system for macromolecular structure solution. *Acta Crystallogr. D.* **66,** 213–221
44. Kabsch, W., and Sander, C. (1983) Dictionary of protein secondary structure: pattern recognition of hydrogen-bonded and geometrical features. *Biopolymers* **22,** 2577–2637

Dynamic feature of mitotic arrest deficient 2–like protein 2 (MAD2L2) and structural basis for its interaction with chromosome alignment–maintaining phosphoprotein (CAMP)

Kodai Hara, Shota Taharazako, Masanori Ikeda, Hiroki Fujita, Yoshiko Mikami, Sotaro Kikuchi, Asami Hishiki, Hideshi Yokoyama, Yoshinobu Ishikawa, Shin-ichiro Kanno, Kozo Tanaka and Hiroshi Hashimoto

J. Biol. Chem. 2017, 292:17658-17667.
doi: 10.1074/jbc.M117.804237 originally published online September 8, 2017